PAPER

A quartz-based micro catalytic methane sensor by high resolution screen printing

IOP Publishing Journal of Micromechanics and Microengineering
J. Micromech. Microeng. **26** (2016) 025021 (10pp) doi:10.1088/0960-1317/26/2/025021

A quartz-based micro catalytic methane sensor by high resolution screen printing

Wenshuai Lu[1], Gaoshan Jing[1], Xiaomeng Bian[1], Hongyan Yu[1] and Tianhong Cui[1,2]

[1] State Key Laboratory of Precision Measurement Technology and Instruments, Department of Precision Instruments, Tsinghua University, Beijing, 100084, People's Republic of China
[2] Department of Mechanical Engineering, University of Minnesota, Minneapolis, MN 55455, USA

E-mail: tcui@me.umn.edu

Received 16 August 2015, revised 7 November 2015
Accepted for publication 24 November 2015
Published 14 January 2016

Abstract

A micro catalytic methane sensor was proposed and fabricated on a bulk fused quartz substrate using a high resolution screen printing technique for the first time, with reduced power consumption and optimized sensitivity. The sensor was designed by the finite element method and quartz was chosen as the substrate material and alumina support with optimized dimensions. Fabrication of the sensor consisted of two MEMS processes, lift-off and high resolution screen printing, with the advantages of high yield and uniformity. When the sensor's regional working temperature changes from 250 °C to 470 °C, its sensitivity increases, as well as the power consumption. The highest sensitivity can reach 1.52 mV/% CH_4. A temperature of 300 °C was chosen as the optimized working temperature, and the sensor's sensitivity, power consumption, nonlinearity and response time are 0.77 mV/% CH_4, 415 mW, 2.6%, and 35 s, respectively. This simple, but highly uniform fabrication process and the reliable performance of this sensor may lead to wide applications for methane detection.

Keywords: methane sensor, screen printing, MEMS

(Some figures may appear in colour only in the online journal)

1. Introduction

Methane is a colorless, odorless and flammable gas widely distributed in nature, and methane leakage detection is crucial in various industrial fields, such as coal mining and natural gas pipeline operation. Additionally, the greenhouse effect caused by methane is 20 times higher than that caused by carbon dioxide [1]. Therefore, a range of methane detection sensors based on different techniques have been developed since the last century, including catalytic combustion [2, 3], metal oxide semiconductor sensing [4, 5], thermal conductivity [6, 7], electrochemical reaction [8], and infrared light absorption [9, 10]. Among these sensors, catalytic combustion sensors (so called 'pellistors') are widely commercialized due to their advantages of simple structure, small size, low cost, and relatively high sensitivity [11]. In principle, a traditional catalytic combustion sensor is composed of a pair of sensing and reference elements ('pellistors') [12]. When heated to a working temperature of around 400 °C to 500 °C [13], with the existence of a noble metal catalyst such as platinum or palladium, the sensing element's temperature will increase due to the catalytic combustion reaction of methane, while the temperature of the reference element (without a catalyst) remains unchanged. The temperature difference between the two elements will correlate linearly with methane concentration. However, the tedious processes of fabricating commercial pellistors is rarely carried out automatically and is mostly needs to be completed by hand, leading to a high labor cost and low repeatability between sensors [12]. This makes it extremely challenging to integrate with an IC detection circuit for large scale applications [14].

Silicon-based micro catalytic sensors have been reported using conventional micro fabrication techniques and show potential for replacing traditional bulk pellistors as they have the advantages of lower power consumption and higher uniformity [12]. Their sensing and reference elements consist of several layers which form a micro hotplate structure, including a dielectric substrate, a heating electrode and an insulating

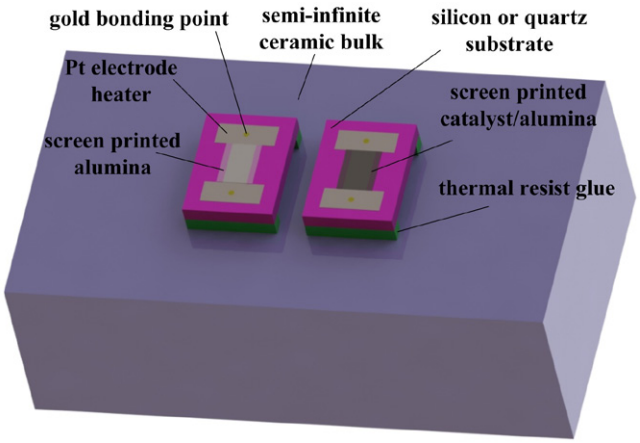

Figure 1. Schematic diagram of the proposed quartz-based catalytic combustion methane sensor consisting of two parts, one sensing element and one reference element, which are placed on two glass mounting gaskets surrounded by an ambient air environment.

dielectric supporting layer. For the sensing element, an additional catalyst is fabricated and dispersed into the dielectric support for a catalytic combustion reaction. Due to silicon's large thermal conductivity coefficient (149 W $m^{-1}{\cdot}K^{-1}$), micro hotplates with suspended membrane structures were fabricated to reduce power consumption [15]. For instance, Park *et al* [16] fabricated a catalytic sensor on a 900 nm thick silicon nitride/ silicon oxide/ silicon nitride membrane by the LPCVD and wet etching process. Then a platinum heating electrode 1 μm thick and an insulating alumina layer were deposited sequentially on top of the membrane. For the sensing element, a thin platinum catalyst layer of less than 20 nm was evaporated on the alumina support. The power consumption of this sensor is about 400 mW, with a sensitivity to methane of 2.2 mV/vol.% CH_4. When the catalyst layer's surface area was increased by electroplating a porous palladium catalyst film, the sensor's sensitivity could reach 12 mV/vol.% CH_4 [12]. In the meantime, a porous alumina-supported palladium catalyst layer was fabricated on the membrane by sol-gel and manual dropping process to increase the sensor's sensitivity to 18 mV/vol.% CH_4 [17]. Nevertheless, these silicon-based sensors all have a suspended membrane (usually around 1 μm thick) structures to offset the massive thermal loss induced by bulk silicon substrates. The complexity of fabricating such silicon-based membrane micro hotplate structures would greatly limit the application of these sensors [18].

In this paper, we proposed a novel design of micro catalytic combustion methane sensor fabricated on a bulk fused quartz substrate without a conventional silicon-based suspended membrane structure. This is an extended version of the work originally reported in 18th International Conference on Solid-State Sensors, Actuators and Microsystems (Transducers 2015) [19]. The sensor's heating electrode was fabricated by the lift-off process and dielectric alumina support was fabricated by high resolution screen printing. The finite element method (FEM) modelling and simulation were utilized to select quartz substrate material with an appropriate thickness. The designated region of alumina supported catalyst can undergo 550 °C, with the central temperature up to 780 °C, without structural failure. The sensor shows a linear response to methane with the concentration from 0 to 2.5 vol.%. Its sensitivity increases as temperatures change from 250 °C to 470 °C, and at its highest point is 1.52 mV/vol.% CH_4, with the power consumption of sensor/compensator element pairs increasing from 344 mW to 720 mW. At 300 °C, the sensitivity is 0.77 mV/vol.% CH_4 and power consumption is about 415 mW. After aging for 14 h in a 0.6% methane environment, the sensitivity decreased slightly to 0.69 mV/% CH_4, while demonstrating better linearity of 2.3%. This simple, but highly uniform fabrication process and the reliable performance of this sensor may lead to wide applications in various industrial fields for detecting combustible gas.

2. Materials and methods

2.1. FEM design and simulation

The micro catalytic sensor was designed and simulated by COMSOL Multiphysics software (COMSOL Inc., CA). As shown in figure 1, a schematic diagram of the sensor consists of two parts, one sensing element and one reference element surrounded by ambient air. For the sensing element, a platinum heating electrode with a layer of γ-alumina and two gold bonding points on top of the electrode is placed on a bulk substrate, with adjustable material and thickness. The bulk substrate material will be compared between silicon and quartz with thickness varying from 50 to 1000 μm. A semi-infinite bulk with a thermal insulation is introduced to simulate the ceramic socket package of the sensor [20]. A tunable DC driving voltage is applied to the bonding pads of the sensing element. For the reference element, all the designs and configurations are identical to the sensing element, except there is no DC driving voltage. Physics models, including Heat Transfer in Solid and Electric Current, are coupled into Multiphysics of Electromagnetic Heat Source. The whole model is surrounded by air with the Convective Heat Flux boundary condition. The relation between the sensor's power consumption and several parameters is investigated, including substrate material, substrate thickness, and alumina support area. The quantity of the catalyst dispersed in alumina support is not considered to simplify the simulation process because of its relatively low loading percentage (5.0 wt.%). It should be noted that the electrodes of sensing and reference elements shown in figure 1 were designed as a rectangular pattern to reduce meshing complexity during numerical simulation, which will demonstrate a similar relation between heating power and working temperature for the fabricated square wave pattern electrodes shown in figure 2. Finally, the simulation results would be the guideline for the following sensor design and fabrication.

2.2. Device fabrication

The micro fabrication processes of the micro catalytic sensor are illustrated in figure 2(a). First, a negative photoresist (NR9-1500PY) was spin-coated at 3000 rpm for 30 s to obtain a 1.5 μm thick film on a 100 μm thick four inch fused quartz wafer (figure 2(a)). After prebaking at 120 °C for

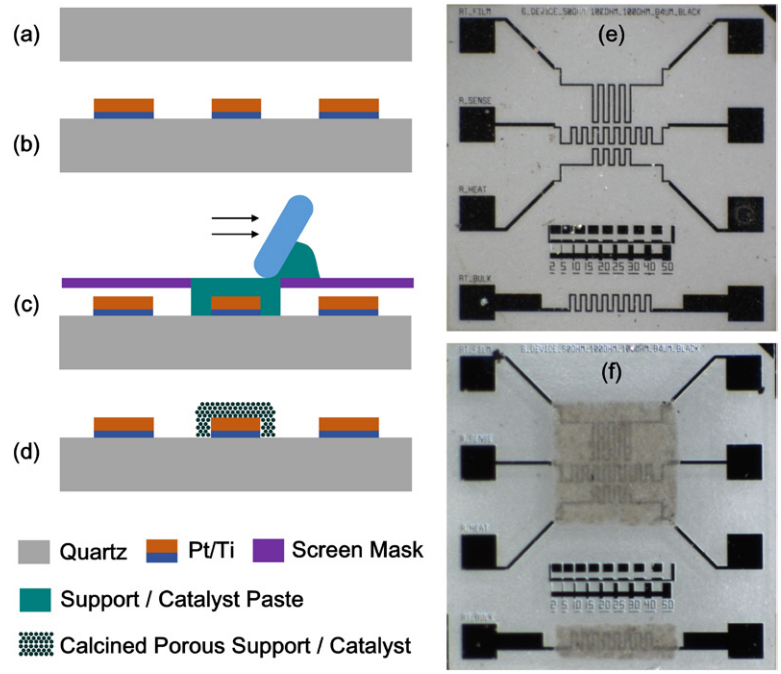

Figure 2. (a) Scheme of the fabrication process for the catalytic methane sensor including (a) 100 μm thick bulk quartz substrate, (b) depositing of heating/sensing electrodes by lift-off, (c) high resolution screen printing of alumina supported catalyst, and (d) calcining of the printed paste to form porous supported catalyst. Optical images of (e) a single sensing element with four square wave pattern electrodes, and (f) a single sensing element with screen printed alumina paste covering the electrodes.

150 s, the photoresist was exposed to UV light for 13.4 s using an EV620 mask aligner (EV Group Inc., NY) and developed for 21 s. Second, 50 nm titanium and 400 nm platinum were sequentially sputtered on the surface, followed by a lift-off process performed in acetone solution (figure 2(b)). Third, a high resolution screen printer (MT650, Micro-tec Co., Ltd., Chiba, Japan) was utilized to generate sensing/reference elements. For a sensing element, a layer of 10 μm porous alumina supported platinum catalyst was patterned on top of heating electrodes by screen printing a paste mixed with alumina and platinum (figure 2(c)). This was synthesized by Shenzhen Senlont Electronic Co., Ltd., using commercialized alumina mixed with platinum catalyst powder (5.0 wt.%, Sigma Aldrich). For a reference element, the silk printing process is the same, except the paste applied was made by pure alumina paste without catalytic metal (Shenzhen Senlont Electronic Co., Ltd.). Last, quartz wafers with the printed paste patterns were dried in an oven at 150 °C for 30 min to remove organic solvent of the paste, and calcined in a muffle furnace at 500 °C for 2 h to form a porous γ-Al_2O_3 supported catalyst layer (figure 2(d)).

As shown in figure 2(e), there are four independent square wave pattern electrodes fabricated in a single sensing element. Three electrodes are covered by a 600 μm by 600 μm rectangular pattern alumina, while the other electrode is covered by a 600 μm by 200 μm rectangular pattern alumina as shown in figure 2(f). Every electrode can be utilized for heating and temperature sensing concurrently. For heating, the electrode is powered to make the catalyst work at a proper working temperature. Simultaneously, an exact working temperature is derived and calculated by temperature coefficient resistance (TCR) deduction of the electrode.

Finally, a 1.5 μm thick photoresist was coated on the quartz wafer at 3000 rpm to prevent scratching during the following dicing process. The whole wafer (figure 3(a)) was cut into 1800 highly uniform single elements (2 mm by 2 mm) by a dicing saw (DAD-321, Disco, Japan). Each element was packaged into a SOP8 socket by gold ball bonding and thermal resist glue to form a micro catalytic sensor (figure 3(b)). Eventually, this sensor was integrated into a tunable constant current bridge circuit PCB for gas sensing measurement as shown in figure 3(c).

2.3. Thermal, electrical and surface properties characterization

Thermal-electrical properties of the micro catalytic sensor were characterized by TCR deduction and infrared imaging technique. To perform TCR deduction, the TCR of the Ti/Pt heating electrode was measured beforehand. First, a micro catalytic sensor was put onto a hotplate, with the temperature changing from 50 °C to 300 °C and exact temperature values were measured by an external thermal couple (TES1307, TES Electrical Electronic Crop., Taiwan). The resistance of the electrode was measured using a data acquisition system (Agilent 34972A, Keysight Technologies, Inc., CA). The sensor's TCR was calculated by equation (1), as well as the sensor's power consumption,

$$R = R_0 \times [1 + \alpha(T - T_0)] \quad (1)$$

where T_0 is the initial temperature at room environment (25 °C), T is the temperature by Joule heating, R_0 is the heater's resistance at T_0, R is the heater's resistance at T, and α is the TCR of the heater. Once the TCR of the Ti/Pt electrode was obtained, a tunable heating power of 30–550 mW was

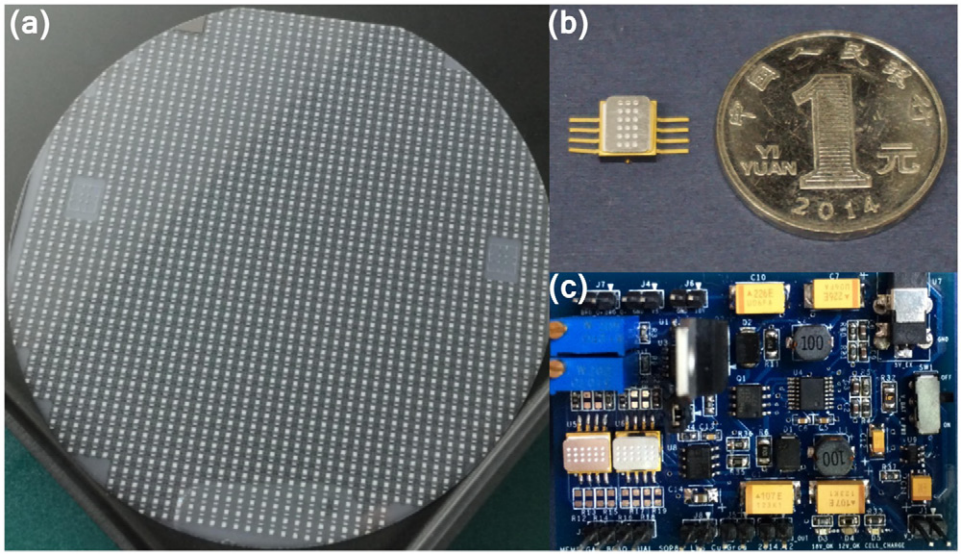

Figure 3. Images of process from micro fabricated sensing/reference elements to integrated methane measurement system. (a) 4 inch quartz wafer with 1800 reference elements screen printed on the heating electrodes after calcining. (b) Packaged sensor with single sensing/reference element in SOP8 socket. (c) Integrated measurement system on PCB.

applied to the heating electrode. From the measured resistance, the average temperature of the heating electrode could be deduced from equation (1), reversely.

By using an infrared imaging technique (Infra Tech VC HD Head 880, InfraTec, Dresden, Germany), the surface temperature profile of the alumina support heated by an embedded heating electrode was characterized. The average and maximum temperature of the alumina support's designated region were obtained by infrared image analyzing software (IRBIS3, InfraTec, Dresden, Germany). Meanwhile, the average temperature of the heating electrode was obtained using the sensor's TCR by equation (1) so that the temperature difference between alumina support surface and embedded heating electrode can be compared.

The thickness of the screen printed alumina support was characterized by a 3D Surface Profilometer (Dektak 150, Veeco, USA). The surface properties of the sensor were characterized by scanning electron microscopy (FEI Quanta 200, Oregon, USA), with a detector enabling energy-dispersive x-ray spectroscopy analysis to verify the composition of alumina supported catalyst. EDS raw data was processed by software of OriginLab.

2.4. Sensor performance characterization

The packaged micro sensor was then integrated into an embedded measurement system. The system consists of a DC constant current bridge amplified by 100 × and a wireless MCU to transform the measured result into a digital signal and transmit by a RF module. The output wireless signal response to the gas was recorded by a wireless PC computer terminal which operated a customized Lab Windows/CVI automatic measurement program. The measurement system was fitted into a customized 15L chamber with a gas delivering module, through which methane concentration can be adjusted from 0 to 3.0%. The outlet of the chamber was connected to an infrared online gas analyzer for methane concentration calibration (Ultramat-23, SIEMENS, Munich, Germany). The sensor's working temperature was precisely tuned by adjusting the constant current. The output of the sensor circuit was recorded by a wireless controlled data acquisition system. The whole experimental setup is illustrated in figure 4, including the gas delivering system, calibrating system, and a data recording system.

3. Results and discussion

3.1. Thermal-electrical and material properties of the micro catalytic sensor

Thermal-electrical properties of the micro catalytic sensor were investigated by FEM simulation, TCR deduction, and infrared imaging. From the simulation results shown in figure 5(a), the temperature distribution profile on a silicon substrate is uniform due to its high thermal conductivity of 149 W $m^{-1}\cdot K^{-1}$, while the profile on a quartz substrate is concentrated in a designated heating area due to quartz's low thermal conductivity of 1.2 W $m^{-1}\cdot K^{-1}$, which is in good accordance with the measured infrared thermal image shown in figure 5(b). The difference between these two profiles implies distinct substrate/ambient environment temperature gradients between silicon and quartz, which affects convective flux and thermal conduction on the substrate interface [21]. The different temperature gradient for silicon and quartz substrate result in differing heat loss and sensor power consumption. As shown in figure 5(c), the power consumption of a silicon sensor (red curve) working at 400 °C is significantly higher than that of a quartz sensor (blue curve). For instance, for a quartz sensor with thickness of 100 μm, it is 504 mW, while for a silicon sensor it is over 3.0 W. Furthermore, for quartz-based sensors with thickness decreasing from 1000 μm to 100 μm, the power consumption drops from 1.2 W to 504 mW. In contrast, for silicon-based sensors with thicknesses

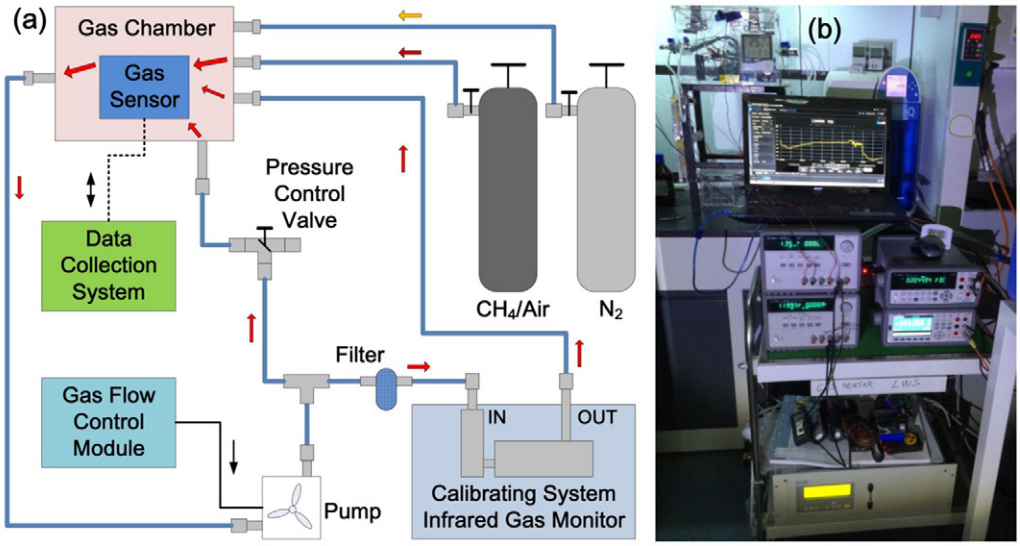

Figure 4. Images of the experiment setup including a gas chamber, a gas delivering system, a calibrating system, and a data acquisition system.

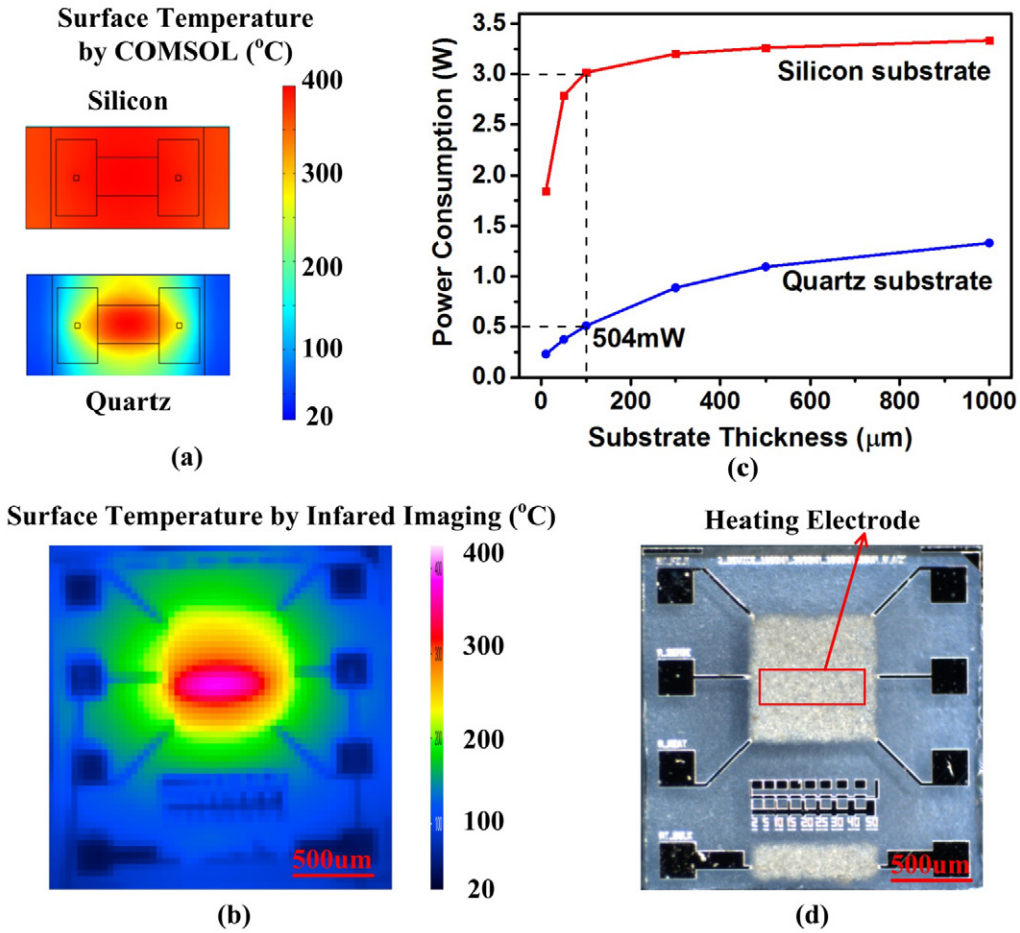

Figure 5. (a) Temperature distribution profiles on silicon and quartz substrates by COMSOL simulation. (b) Temperature distribution profiles of a quartz sensor by infrared imaging. (c) Power consumption versus thicknesses of silicon and quartz substrates by COMSOL. (d) Optical image of a sensor reference element and heating electrode.

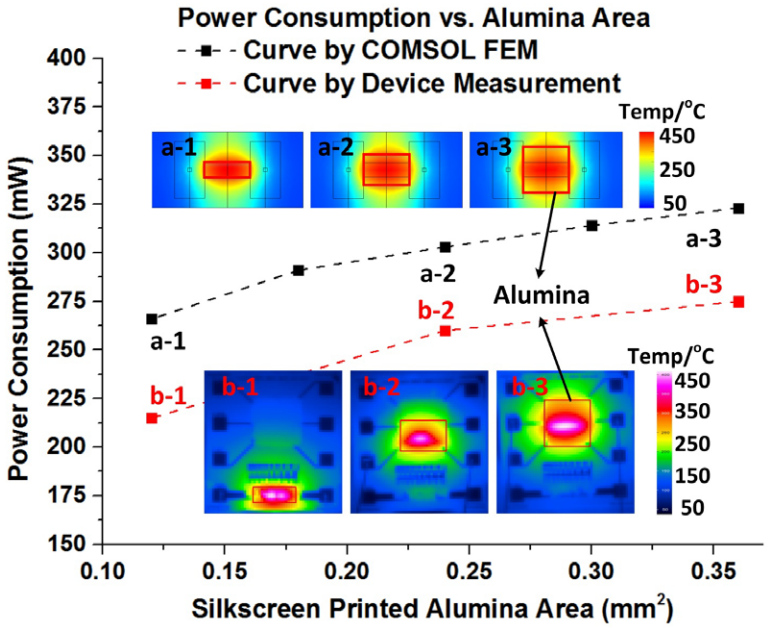

Figure 6. Curves and temperature distribution profiles of screen printed alumina area versus power consumption by FEM simulation (a-1)–(a-3) and device measurement (b-1)–(b-3).

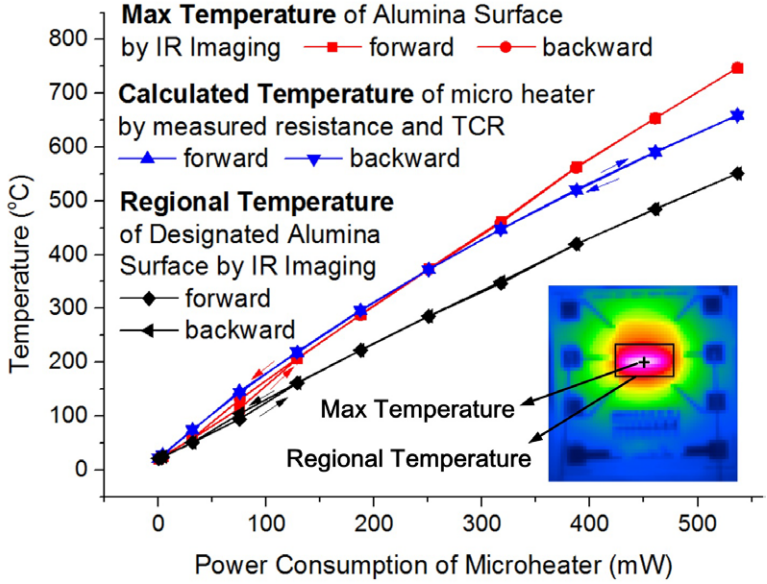

Figure 7. Testing results of high temperature thermal stability of the sensor structure by increasing and decreasing self-heat power supply, including curves of surface regional (black) and maximum (red) temperature measured by infrared imaging, and average (blue) temperature of micro heater calculated by measured TCR and resistance of the electrodes. Every point lasts for at least 30 min.

decreasing from 1000 μm to 100 μm, the power consumptions only reduce from 3.2 W to 3.0 W. For the sake of sensor power consumption reduction and material availability, we chose 100 μm thick quartz substrates for fabricating micro catalytic sensors.

For a quartz-based sensor, the area of the screen printed alumina support on top of the heating electrode also affects the sensor's power consumption. As shown in figure 6, the sensor's power consumption increases from 265 mW to 325 mW as the area of alumina support increases from 0.12 mm^2 to 0.36 mm^2 (black curve, a-1 to a-3) by simulation, which is in good correlation with the trend measured from fabricated devices (red curve, b-1 to b-3). The reason is that thermal conductivity of porous alumina (around 15–20 W m^{-1}·K^{-1} [22]) is much higher than that of quartz. A larger area of porous alumina support would lead to more thermal loss of the sensor. To further reduce the sensor's power consumption, our approach is to keep the area of screen printed alumina aligned with the outline of the heating electrode.

The thermal stability of the micro sensor was also characterized by TCR deduction and infrared imaging. The relation between the three temperatures are investigated, including

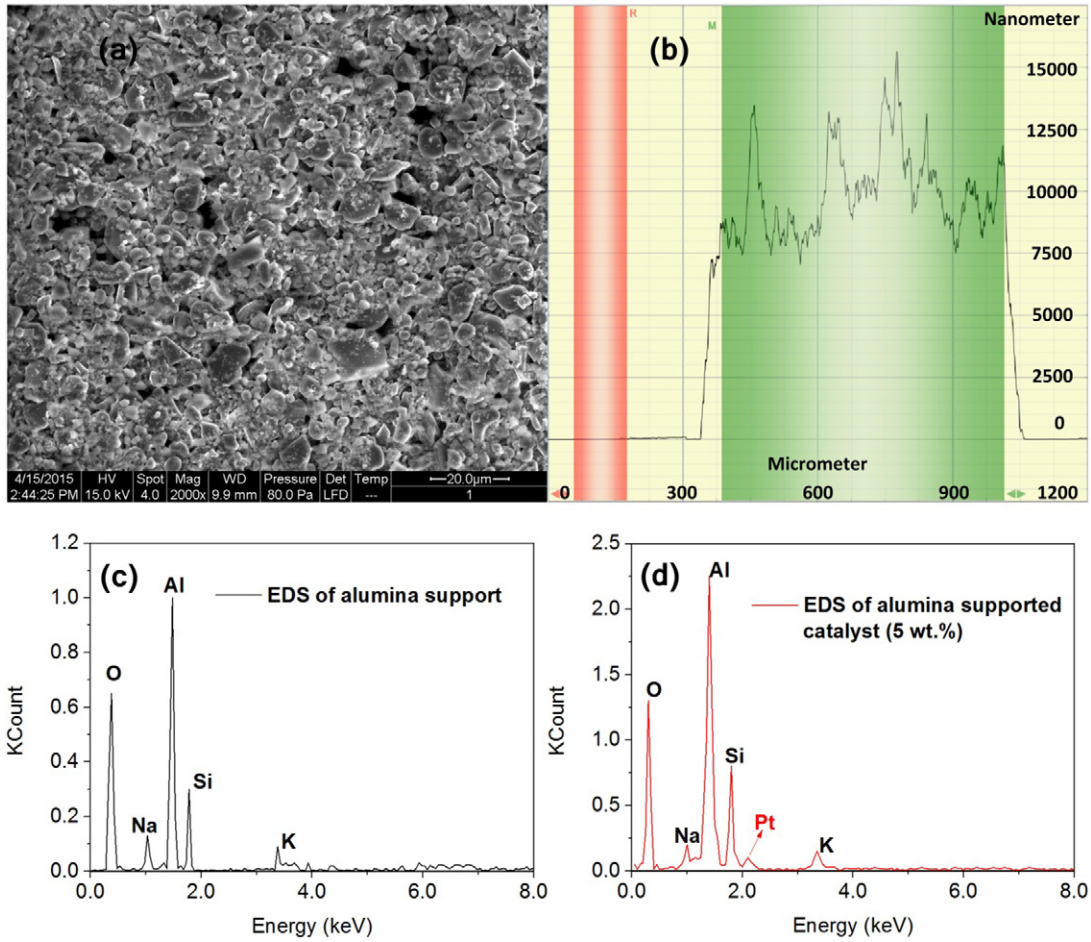

Figure 8. (a) SEM of the screen printed alumina support's surface profile which demonstrated a porous alumina surface with platinum catalyst embedded inside the support. (b) Thickness profile of the printed alumina support by 3D surface profilometer. EDS results of the (c) reference element and (d) sensing element which demonstrate there is no platinum catalyst inside a reference element but roughly 5% of platinum inside a sensing element.

the regional (black curve) and maximum temperatures (red curve) of the alumina surface, and temperature of the heating electrode (blue curve) shown in figure 7. The regional and maximum temperatures of the alumina surface were measured by an external infrared camera, and the temperature of the heating electrode was calculated by it simultaneously acting as a sensing electrode, with the TCR of 2.64×10^{-3}/°C from our measurement. Under the same applied DC power, the maximum temperature of alumina is the highest and the regional temperature by infrared imaging is the lowest due to thermal loss from the sensor to the ambient environment. When a DC power was applied in increasing and decreasing direction, two curves almost coincide with each other, with every test point on these curves lasting for over 30 min. From published results, platinum membrane will degrade and lead to functional failure typically at 500 °C [23], whereas our Ti/Pt heating electrode can stand 650 °C, with the regional temperature of heated alumina up to 550 °C and the maximum temperature up to 780 °C without functional failure, which demonstrates great thermal stability of the micro catalytic sensor.

SEM of the calcined screen printed alumina support's surface profile is shown in figure 8(a), which illustrates a porous alumina surface with a platinum catalyst embedded inside the support. The thickness profile of the screen printed alumina support was shown in figure 8(b) with an average thickness of 9.97 μm, as well as a surface roughness about RMS 2.55 μm. A uniform alumina support was achieved with optimized parameters for the high resolution screen printer. A high resolution screen was used with a mesh count of 500 (500 threads per inch) and a thread diameter of 18 μm. When printing, the pressure applied on a scraper is 0.149 MPa and printing speed is 300 mm s^{-1}. Additionally, $\pm$ 10 μm alignment accuracy can be achieved by this screen printer. Compositions of the reference and sensing elements are shown in figures 8(c) and (d), respectively, which demonstrate there is no platinum catalyst inside a reference element but roughly 5% of platinum inside a sensing element.

3.2. Methane sensing performance

The sensor's response to methane as the temperature varies from 250 °C to 470 °C is demonstrated in figure 9. As the working temperature increases, the linear sensitivity (S) increases as well, from 0.43 mV/% CH_4 to 1.52 mV/% CH_4 without amplification. Meanwhile, the sensor's power consumption also increases from 344 mW to 720 mW for a

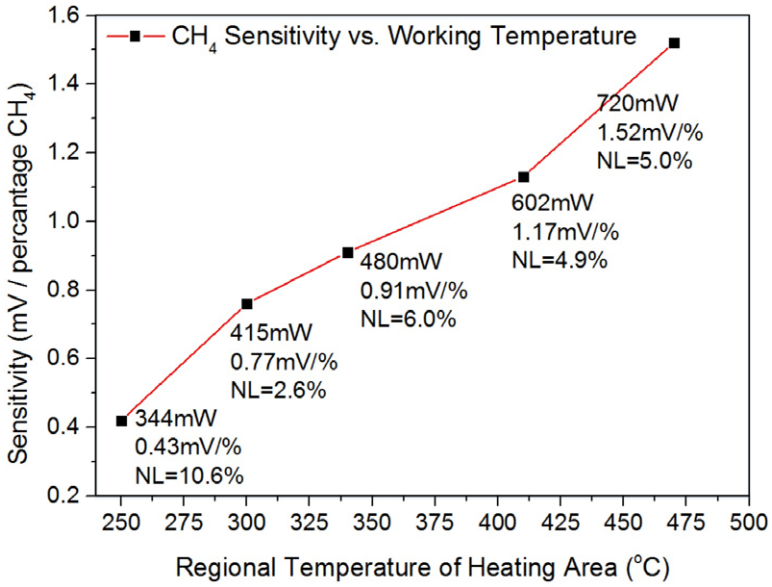

Figure 9. Sensitivity and nonlinearity of the fabricated sensors versus regional working temperatures from 250 °C to 470 °C.

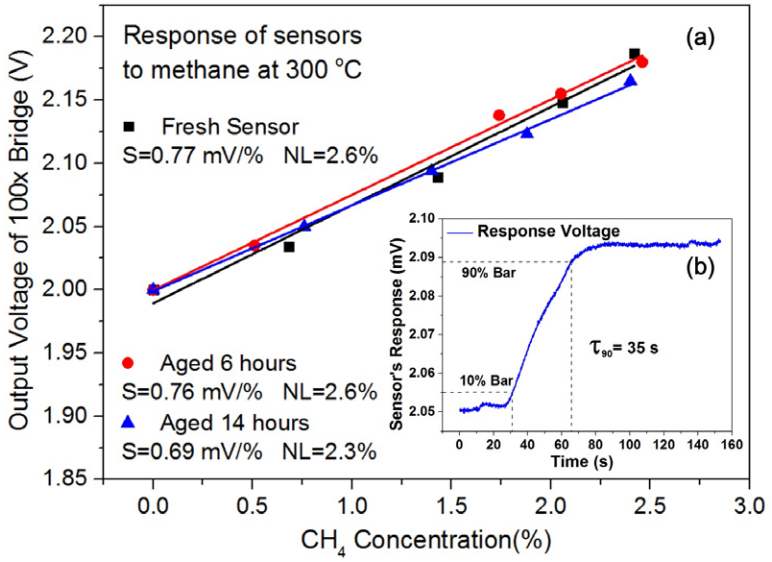

Figure 10. (a) Response to methane from 0 to 2.5% including sensitivity and nonlinearity of fresh sensor, sensor aged in 0.6% methane for 6 h, and sensor aged in 0.6% methane for 14 h. (b) Response time (τ_{90}) of the sensor to methane stepping from 0.75% to 1.40%.

pellistor pair. This change of sensitivity may due to platinum's catalytic activity variation as a function of temperatures [24]. Also, the nonlinearity (NL) of the sensor varies at different working temperatures. A lowest nonlinearity of 2.6% was achieved at working temperature of 300 °C, which was chosen as optimized working temperature for the fabricated sensors, with a decent sensitivity of 0.77 mV/% CH_4 without amplification and power consumption of 415 mW. The relatively low sensitivity may be a result of the low loading content of the catalyst (5.0 wt.%) compared to the designs of other groups , where the content of loaded platinum or palladium is usually around 15 wt.%–40 wt.% [17, 25, 26]. We will further investigate the optimization of the catalyst loading in a future study.

To further optimize the sensor's performance, an aging treatment process is applied to enhance the long time stability of the catalyst. Typically, aging treatment is realized by heating the catalyst at a proper temperature for several hours (usually much longer than calcining period) or by working in a proper concentration of methane [27, 28], to make the active sites of the catalyst more stable [25]. Here, the aging treatment is executed by fitting the sensor system in 0.6% methane for 6 and 14 h, and the response of the aged sensors to methane of 0% to 2.5% was measured. As shown in figure 10(a), the sensitivity exhibits a negligible decrease from 0.77 mV/% CH_4 to 0.76 mV/% CH_4 after 6 h aging, and slight decrease to 0.69 mV/% CH_4 after further additional 8 h aging. In contrast, the sensor's nonlinearity improves by dropping from 2.6% to 2.3% after 14 h aging. No drastic decrease of the sensitivity was observed during the test, which further indicates the good thermal stability of the screen printed supported catalyst [25].

The sensor's gas sensing profile is shown in figure 10(b) and the 90% response time to methane with a concentration step from 0.75% to 1.40% was derived as 35 s.

4. Conclusion

A novel design of micro catalytic combustion methane sensor fabricated on a bulk fused quartz substrate without a conventional silicon-based suspended membrane structure was proposed and fabricated uniformly by simple lift-off Ti/Pt electrodes and high resolution screen printing alumina supported 5.0 wt.% Pt catalyst. Finite element method (FEM) modelling and simulation was utilized to verify the effect of low thermal conductivity of substrate material and optimize the thickness of the quartz substrate, together with the area of screen printed alumina, which shows perfect accordance with actual measurements. The designated region of alumina supported catalyst can withstand 550 °C with the central temperature achieving up to 780 °C without structural failure. The sensor shows a linear response to methane with the concentration from 0 to 2.5 vol.%. The sensitivity increases from 0.43 mV/% to 1.52 mV/% CH_4 as the working temperature increases from 250 °C to 470 °C, with the power consumption of sensor/compensator element pairs increasing from 344 mW to 720 mW. A temperature of 300 °C was chosen as the optimized working temperature with the sensor's sensitivity of 0.77 mV/% CH_4 and power consumption of 415 mW together with a lowest nonlinearity of 2.6%. By further aging for 14 h in 0.6% methane, the sensor's sensitivity decreases slightly to 0.69 mV/% CH_4, while the nonlinearity decreases to 2.3%. The response time of the sensor is 35 s. This simple, but highly uniform fabrication process and reliable performance of this sensor may lead to wide applications in various industrial fields for detecting combustible methane.

Acknowledgments

The work of this paper is partly supported by Shanxi Chuangqi Co. Ltd. The authors also thank Y Peng, T Zeng, Beijing Capitalbio Co. Ltd., Kunshan SIBCO Co. Ltd., and the Engineering Research Center for Navigation Technology at Tsinghua University for the provision of related micro machining and characterization services.

References

[1] Cargnello M, Jaén J J D, Garrido J C H, Bakhmutsky K, Montini T, Gamez J J C, Gorte R J and Fornasiero P 2012 Exceptional activity for methane combustion over modular Pd @ CeO_2 subunits on functionalized Al_2O_3 *Science* **337** 713–7

[2] Wang Y, Tong M M, Zhang D and Gao Z 2010 Improving the performance of catalytic combustion type methane gas sensors using nanostructure elements doped with rare earth cocatalysts *Sensors* **11** 19–31

[3] Yunusa Z, Hamidon M N, Kaiser A and Awang Z 2014 Gas sensors: a review *Sensors Transducers* **168** 61–75

[4] Liu Y, Koep E and Liu M 2005 A highly sensitive and fast-responding SnO_2 sensor fabricated by combustion chemical vapor deposition *Chem. Mater.* **17** 3997–4000

[5] Rahmani M B, Keshmiri S H, Yu J, Sadek A Z, Al-Mashat L, Moafi A, Latham K, Li Y X, Wlodarski W and Kalantar-zadeh K 2010 Gas sensing properties of thermally evaporated lamellar MoO_3 *Sensors Actuators* B **145** 13–9

[6] Xibo D, Xiaoyan G, Yuechao C, Xue S and Zhaoxia L 2013 Study on thermal conductivity methane sensor constant temperature detection method *Telkomnika* **11** 725–32

[7] Tardy P, Coulon J-R, Lucat C and Menil F 2004 Dynamic thermal conductivity sensor for gas detection *Sensors Actuators* B **98** 63–8

[8] Zaromb S, Otagawa T and Stetter J R 1986 Method of determining methane and electrochemical sensor therefor *US Patent* 4591414

[9] Chen C, Newcomb R W and Wang Y 2013 A trace methane gas sensor using mid-infrared quantum cascaded laser at 7.5 μm *Appl. Phys.* B **113** 491–501

[10] Shemshad J 2013 Design of a fibre optic sequential multipoint sensor for methane detection using a single tunable diode laser near 1666 nm *Sensors Actuators* B **186** 466–77

[11] Karpova E, Mironov S, Suchkov A, Karelin A, Karpov E E and Karpov E F 2014 Increase of catalytic sensors stability *Sensors Actuators* B **197** 358–63

[12] Bartlett P N and Guerin S 2003 A micromachined calorimetric gas sensor: an application of electrodeposited nanostructured palladium for the detection of combustible gases *Anal. Chem.* **75** 126–32

[13] Neyestanaki A K, Klingstedt F, Salmi T and Murzin D Y 2004 Deactivation of postcombustion catalysts, a review *Fuel* **83** 395–408

[14] Fischer A, Forsberg F, Lapisa M, Bleiker S, Stemme G, Roxhed N and Niklaus F 2015 Integrating MEMS and ICs *Microsyst. Nanoeng.* **1** 15005

[15] Lee K-N, Lee D-S, Jung S-W, Jang Y-H, Kim Y-K and Seong W-K 2009 A high-temperature MEMS heater using suspended silicon structures *J. Micromech. Microeng.* **19** 115011

[16] Lee J S, Park J W and Shin S M 1997 Fabrication of a micro catalytic gas sensor using thin film process and Si anisotropic etching techniques *Sensors Actuators* B **45** 265–9

[17] Xu L, Wang Y, Zhou H, Wang Y, Liu Y, Li T and Wang Y 2012 Design, fabrication, and characterization of a high-heating-efficiency 3D microheater for catalytic gas sensors *J. MEMS.* **21** 1402–9

[18] Shin W, Nishibori M, Houlet L F, Itoh T, Izu N and Matsubara I 2009 Fabrication of thermoelectric gas sensors on micro-hotplates *Sensors Actuators* B **139** 340–5

[19] Lu W, Jing G, Bian X and Cui T 2015 Micro catalytic methane sensor on bulk quartz substrate *Proc. Transducers* (*Anchorage, USA, 21–25 June 2015*) pp 1495–8

[20] Min Y J, Palisoc A L and Lee C C 1990 Transient thermal study of semiconductor devices *IEEE Trans. Compon. Hybrids Manuf. Technol.* **13** 980–8

[21] Salomons S, Hayes R E, Poirier M and Sapoundjiev H 2004 Modelling a reverse flow reactor for the catalytic combustion of fugitive methane emissions *Comput. Chem. Eng.* **28** 1599–610

[22] Auerkari P 1996 Mechanical and physical properties of engineering alumina ceramics *Technical Research Center of Finland, VTT Tiedotteita-Meddelanden-Research Notes 1792* (www.vtt.fi/inf/pdf/tiedotteet/1996/T1792.pdf)

[23] Tiggelaar R M, Sanders R G P, Groenland A W and Gardeniers J G E 2009 Stability of thin platinum films implemented in high-temperature microdevices *Sensors Actuators* A **152** 39–47

[24] Persson K, Ersson A, Jansson K, Fierro J L G and Järås S G 2006 Influence of molar ratio on Pd-Pt catalysts for methane combustion *J. Catal.* **243** 14–24

[25] Nishibori M, Shin W, Tajima K, Houlet L F, Izu N, Itoh T and Matsubara I 2008 Long-term stability of Pt/alumina catalyst combustors for micro-gas sensor application *J. Eur. Ceram. Soc.* **28** 2183–90

[26] Liu F, Zhang Y, Yu Y, Xu J, Sun J and Lu G 2011 Enhanced sensing performance of catalytic combustion methane sensor by using Pd nanorod/γ-Al_2O_3 *Sensors Actuators* B **160** 1091–7

[27] Wang Y, Tong M M, Zhang Dan and Gao Z 2011 Improving the performance of catalytic combustion type methane gas sensors using nanostructure elements doped with rare earth cocatalysts *Sensors* **11** 19–31

[28] Nagai Y, Hirabayashi T, Dohmae K, Takagi N, Minami T, Shinjoh H, Shin M 2006 Sintering inhibition mechanism of platinum supported on ceria-based oxide and Pt-oxide-support interaction *J. Catal.* **242** 103–9